Nuclear Spin Relaxation of Longitudinal and Singlet Order in Liquid-CO$_2$ Solutions

Aliki Moysiadi[†], Francesco Giustiniano[†], Andrew M. R. Hall[†], Topaz A. A. Cartlidge, Lynda J. Brown and Giuseppe Pileio*

School of Chemistry, University of Southampton, Southampton, United Kingdom

Hyperpolarization techniques can enormously enhance the NMR signal thus allowing the exploitation of hyperpolarized substrates for *in-vivo* MRI applications. The short lifetime of hyperpolarized spin order poses significant limitations in such applications. Spin order storage can be prolonged through the use of long-lived spin states. Additionally, the storage of spin polarization–either in the form of longitudinal or singlet order–can be prolonged in low viscosity solutions. Here, we report the use of low viscosity liquid-CO$_2$ solutions to store nuclear spin polarization in the form of longitudinal and singlet order for extended periods. Our results demonstrate that this storage time can be considerably sustained in liquid-CO$_2$ solutions in comparison to other low viscosity solvents, opening up the possibility of new, exciting storage experiments in the future.

Keywords: singlet spin order, liquid-CO$_2$, nuclear magnetic resonance, long-lived spin states, nuclear spin relaxation

INTRODUCTION

Molecules that contain an "isolated" spin-1/2 pair of nuclei, offer the possibility to prepare a form of spin order, namely, singlet spin order (Carravetta and Levitt, 2004; Carravetta et al., 2004; Pileio, 2020) with the fundamental property of being long-lived. This is due to the fact that singlet spin order decays at a much slower rate than the longitudinal spin order conventionally used in most NMR experiments. This form of order has already been used in a range of different applications including: high-sensitivity quantification of ligand binding (Salvi et al., 2012; Buratto et al., 2014); measurements of slow translational dynamics (Cavadini et al., 2005; Ahuja et al., 2009; Dumez et al., 2014; Pileio et al., 2015; Pileio and Ostrowska, 2017; Tourell et al., 2018); and long-lived molecular tags to preserve information over a long time (DeVience et al., 2013; Feng et al., 2013; Zhang et al., 2014, 2015, 2016; Dumez et al., 2015; Theis et al., 2016; Mamone and Glöggler, 2018; Saul et al., 2019; Tanner et al., 2019; Yang et al., 2019). There is great potential for exploitation of long-lived spin order in high impact applications and in combination with techniques such as PHIP (Bowers and Weitekamp, 1987), SABRE (Adams et al., 2009), and dissolution-DNP (Ardenkjaer-Larsen et al., 2003) as a vehicle to preserve spin hyperpolarization. In the important fields of *in-vivo* MRI and molecular imaging, it is crucial to achieve the signal enhancement provided by such techniques. The capacity to preserve such enhancement for very long time periods so as to allow quality controls, transport and injection into the patient offers an exciting step forward. Moreover, the possibility to preserve hyperpolarization for hour-long periods would allow delocalisation of the point-of-production (the hyperpolarization equipment) from the point-of-use (the NMR/MRI machine). This presents many advantages but perhaps the most important is that the point-of-use does not necessarily need to be equipped with hyperpolarizer instrumentation and have specially trained personnel (in the case of dissolution-DNP this is very costly).

Recent progress in this field exploits the use, at the hyperpolarization stage, of radical-containing porous matrices that allow the storage of hyperpolarized longitudinal order in the form of a frozen solid which also displays very long lifetimes (Gajan et al., 2014).

Another possible way to achieve this decentralization involves the exploitation of long-lived spin states. Indeed, long-lived spin order with record lifetimes of 70 min in degassed acetone-d_6 solutions at 20°C and 0.4 T field (Stevanato et al., 2015) and of 108 min at 30°C and 0.25 T field (Hall et al., 2020) have been reported. However, in general, the conditions which maximize the lifetime may be different to the conditions required at usage. For example, storage in a low-viscosity solvent such as acetone can prolong the lifetime of those states, but such solvent is clearly incompatible for use in a clinical setting.

The rationale behind why the lifetime of spin order can be prolonged in low-viscosity media arises from the very core of nuclear spin relaxation theory (Kowalewski and Mäler, 2006). Spin relaxation is due to fluctuating magnetic fields present in solutions. These fields have a different nature and are ultimately due to spin-spin, spin-field and spin-rotation interactions. The contributions from different mechanisms are additive to the total relaxation rate. Moreover, the spin-spin mechanism due to dipole-dipole interactions between the two spins in the spin-1/2 pair (ipDD) dominates the relaxation rate in the case of longitudinal spin order in degassed samples. The ipDD mechanism, however, does not affect the singlet order lifetime (Levitt, 2012). The spin-field mechanism due to the chemical shift tensor anisotropy (CSA) is, typically, the second in order of importance and affects both longitudinal and singlet order. Spin-rotation mechanisms due either to the coupling between spin and angular moment (SR) or to the coupling between spin and internal motions (SIM) are the next in terms of importance; all other mechanisms including dipole-dipole interaction with out-of-pair spins, interactions with spins in solvent molecules and so on are of minor importance and can be neglected in a first approximation. A detailed discussion of these mechanisms and their role in singlet order relaxation has been summarized in a book chapter (Pileio, 2020).

The very fact that those magnetic fields fluctuate is due to the dynamics of molecules in solution including rotation, diffusion and collision events. The fundamental parameter used to characterize these fluctuations is the correlation time. The contribution to the total decay rate from ipDD and CSA mechanisms is proportional to a correlation time which is linked to the molecular rotational diffusion. This correlation time is usually indicated as τ_c but differentiated into τ_1 and τ_2 depending on the rank of the interaction (ipDD is a rank-2 interaction while CSA has rank-1 (CSA$^-$) and rank-2 (CSA$^+$) components). Both τ_1 and τ_2 are directly proportional to viscosity. Conversely, the contribution to the total decay rate from spin-rotation mechanisms is directly proportional to a correlation time which is linked to molecular collision. This correlation time is usually indicated as τ_{SR} but is inversely proportional to viscosity. This means that, depending on the relative strength of the active interactions, the longitudinal and singlet order lifetimes can be extended by reducing the viscosity of the solution. More

appropriately, this lifetime extension is observed whenever the decay rates are dominated by mechanisms such as ipDD or CSA, whereas the opposite could be observed when SR mechanisms prevails.

As a consequence, we were interested in exploring the use of liquified CO$_2$ gas as a low-viscosity solvent in which spin order can be stored either as longitudinal or singlet order. Pure liquid-CO$_2$ has a viscosity of 0.06 cP which is significantly lower than, for example, pure acetone-d_6 which has a viscosity of 0.34 cP, a factor of ~5.6 times lower. As previously outlined, in situations where ipDD and CSA relaxation mechanisms dominate, an elongation of singlet order lifetime is theoretically possible. A further significant advantage of exploiting liquid-CO$_2$ is the ability to rapidly evaporate this solvent by simply venting the NMR tube, thus allowing easy exchange with another solvent. This would facilitate experiments that employ one set of conditions to prolong the storage of hyperpolarization and other conditions for the time of use.

The use of CO$_2$ as a solvent in NMR is not new (Lamb et al., 1989; Bai et al., 1997; Gaemers et al., 1999; Gaemers and Elsevier, 2000; Yonker, 2000; Khodov et al., 2020) but our contribution is the first report in which the properties of this solvent are investigated in the context of enhancing the lifetime of long-lived spin order.

Herein, we describe equipment built to prepare and handle NMR tubes filled with liquid-CO$_2$ solutions. We present a thorough investigation of the lifetime of longitudinal and singlet spin order in liquid-CO$_2$ solutions as compared with the same values measured in more conventional organic solvents. We report data measured at a wide variety of magnetic fields from 16.4 T to 50 mT for three different molecular systems that all support long-lived spin order. These findings are discussed in terms of a simplified relaxation analysis, based on previously derived analytical equations, and we propose future experiments made possible by our results.

MATERIALS AND METHODS

Instrumentation
Experiments presented in this paper were run on a variety of NMR instruments. Data at 16.4 T was collected on a Bruker 700 MHz Avance Neo spectrometer equipped with a 5 mm TCI prodigy cryoprobe. Data at 11.7 T was collected on a Bruker 500 MHz Avance III spectrometer equipped with a 5 mm TBO Z-gradient probe. Data at 7 T was collected on a Bruker 300 MHz Avance III spectrometer equipped with a Bruker MICWB40 microimaging probe carrying a ^{1}H/^{13}C 10 mm resonator. Data collected at magnetic fields below 7 T was collected in field-cycling mode by using an automatic sample shuttle (Hall et al., 2020) installed on the 300 MHz spectrometer.

Molecular Systems
Experiments have been carried out on a variety of molecular systems which support long-lived spin states. The molecular structures of all systems employed were reported in **Figure 1**. The first molecule is a doubly-^{13}C-labeled and perdeuterated

FIGURE 1 | Structure of the molecular systems employed in this work.
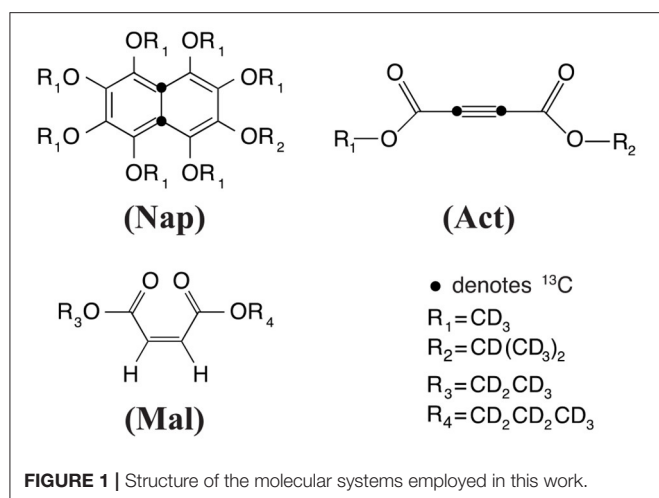
derivative of naphthalene, 1,2,3,4,5,6,8-heptakis(methoxy-d_3)-7-((propan-2-yl-d_7)oxy)-4a,8a-^{13}C$_2$-naphthalene (**Nap**). The second molecule is a doubly-^{13}C-labeled and perdeuterated unsymmetrical diester of acetylene dicarboxylic acid, 1-(methyl-d_3) 4-(propan-2-yl-d_7) but-2-ynedioate (**Act**). The third molecule is a perdeuterated unsymmetrical diester of the maleic acid, 1-(ethyl-d_5)-4-(propyl-d_7)(Z)-but-2-enedioate (**Mal**). All molecules have been synthesized in-house according to published procedures (Pileio et al., 2012; Hill-Cousins et al., 2015; Brown, 2020).

Samples

Molecules **Nap, Act,** and **Mal** have been used to prepare several different samples. For clarity we have labeled all preparations with different names and these are summarized in **Table 1**. The sample nomenclature works as follow: the first three digits reflect the molecular system; the next three digits refer to the solvent in which the molecule has been dissolved; the last digit, when present, distinguishes similar samples prepared at different concentration as detailed in **Table 1**.

Samples were degassed to remove paramagnetic dissolved oxygen. Excluding liquid-CO$_2$ samples, degassing was done by ten freeze-pump-thaw cycles; the degassing procedure used for samples in liquid-CO$_2$ is described below.

High Pressure Tubes and Volume Restriction Inserts

All samples other than those in liquid-CO$_2$ have been prepared in standard 5 or 10 mm LPV NMR tubes. Samples involving liquid-CO$_2$ are prepared in special high-pressure NMR tubes (purchased from Rototec-Spintec, DE) consisting of either a zirconia or sapphire tube connected to an aluminum needle-valve. High pressure tubes (5 mm) made of zirconia can withstand pressures up to 1,000 bar whilst 10 mm high pressure tubes are made of sapphire and can withstand pressures up to 300 bar. To confine the sample within the coil region (so as to minimize the effects of thermal convection) we constructed a glass insert consisting of two precision-manufactured filled glass

rods and a piece of glass tube that fits inside the high-pressure tubes to confine the sample within a 10.5 mm cylindrical chamber placed in the middle of our 18 mm long coil. The insert outer diameter is slightly smaller than the high-pressure tube internal diameter (ID) leaving just a 250 μm gap. Tube construction and all dimensions are illustrated in **Figure 2**.

CO$_2$ Samples Preparation

To allow preparation of samples in liquid-CO$_2$ specialist equipment was required. The apparatus was constructed as diagrammatized in **Figure 3**. The "filling station" works by trapping a known amount of CO$_2$ gas in a cylinder of known volume at room temperature and relatively low pressure, the amount required for a given experiment is then transferred into the high-pressure tube by cryogenic pumping using liquid-N$_2$.

The gas from a N5.0 grade CO$_2$ canister fills a 50 ml vessel at the desired pressure as monitored through a pressure sensor connected to the vessel. The vessel is at room temperature and the exact value of the temperature is measured and noted. The O$_2$ content of the CO$_2$ bottle has been measured to be 1 ppb using a OxyQC Wide Range oxygen meter by Anthon Paar; the gas was nevertheless filtered through a Restek high-capacity oxygen and moisture trap placed between the bottle and the 50 ml vessel to further remove O$_2$. The whole tubing (including vessel and high-pressure tube) is filled with CO$_2$ and evacuated a few times to remove the O$_2$ possibly present in the equipment.

Successively, the desired amount of CO$_2$ gas at the desired pressure is trapped in the 50 ml vessel, from where it is sucked into the high-pressure NMR tube (which already contains a given amount of the desired molecular system) by immersing the tube into the liquid-nitrogen Dewar. The CO$_2$ gas liquifies or solidifies, depending on the exact conditions, inside the high-pressure tube and while under liquid-N$_2$. Once the transfer occurs, the NMR tube needle valve is closed, and the tube is left to equilibrate at ambient temperature. The amount of gas needed to be trapped in the 50 ml vessel ($V_V = 50$ ml) is calculated on the basis of what amount of liquid-CO$_2$ we want/need to fill the high-pressure tube with (Smith et al., 2013). In the preparations below where the high-pressure 10 mm sapphire tube is used, and similarly for the 5 mm zirconia case, our aim is to fill a 10.5 mm long and 5.8 mm ID chamber with liquid-CO$_2$ (details in **Figure 2**). To do that we calculate the volume of liquid CO$_2$ (V_{liq}) as a function of the mass of CO$_2$ (M_{CO_2}) to be trapped in that volume using:

$$V_{liq} = \frac{M_{CO_2} \; \chi_{liq}}{\rho_{liq}} \tag{1}$$

where ρ_{liq} is the density of liquid-CO$_2$ at the measured temperature (T) and the liquid fraction χ_{liq} is calculated once the density of liquid-CO$_2$, the density of gas-CO$_2$ (ρ_{gas}) and the system density (ρ_{sys}) are known:

$$\chi_{liq} = 1 - \frac{\rho_{gas}}{\rho_{sys}} \left(\frac{\rho_{liq} - \rho_{sys}}{\rho_{liq} - \rho_{gas}} \right) \tag{2}$$

$$\rho_{sys} = \frac{M_{CO_2}}{V_t} \tag{3}$$

TABLE 1 | Nomenclature and preparation details of all samples used in the paper.

Sample name	Molecular system	Solvent	Viscosity of pure solvent at 20°C (cP)*	Concentration (mM)
NapCo2a	Nap	liquid-CO$_2$ (Co2)	0.06	36
NapCo2b	Nap	liquid-CO$_2$ (Co2)	0.06	61
NapCo2c	Nap	liquid-CO$_2$ (Co2)	0.06	85
NapCo2d	Nap	liquid-CO$_2$ (Co2)	0.06	108
NapTbu	Nap	t-butanol-d$_{10}$ (Tbu)	4.3	200
NapDms	Nap	DMSO-d$_6$ (Dms)	2.4	200
NapEth	Nap	Ethanol-d$_6$ (Eth)	1.2	150
NapClf	Nap	Chloroform-d (Clf)	0.57	260
NapMet	Nap	Methanol-d$_4$ (Met)	0.52	160
NapAce	Nap	Acetone-d$_6$ (Ace)	0.34	200
NapCo2e	Nap	liquid-CO$_2$ (Co2)	0.06	50
ActClf	Act	Chloroform-d (Clf)	0.57	700
ActCo2	Act	liquid-CO$_2$ (Co2)	0.06	100
MalEth	Mal	Ethanol-d$_6$ (Eth)	1.2	500
MalCo2	Mal	liquid-CO$_2$ (Co2)	0.06	340

*Handbuch der Instrumentellen Analytik NMR-spektroskopie provided by S. Thomas in "Spectroscopic Tools" URL: http://www.science-and-fun.de/tools/.
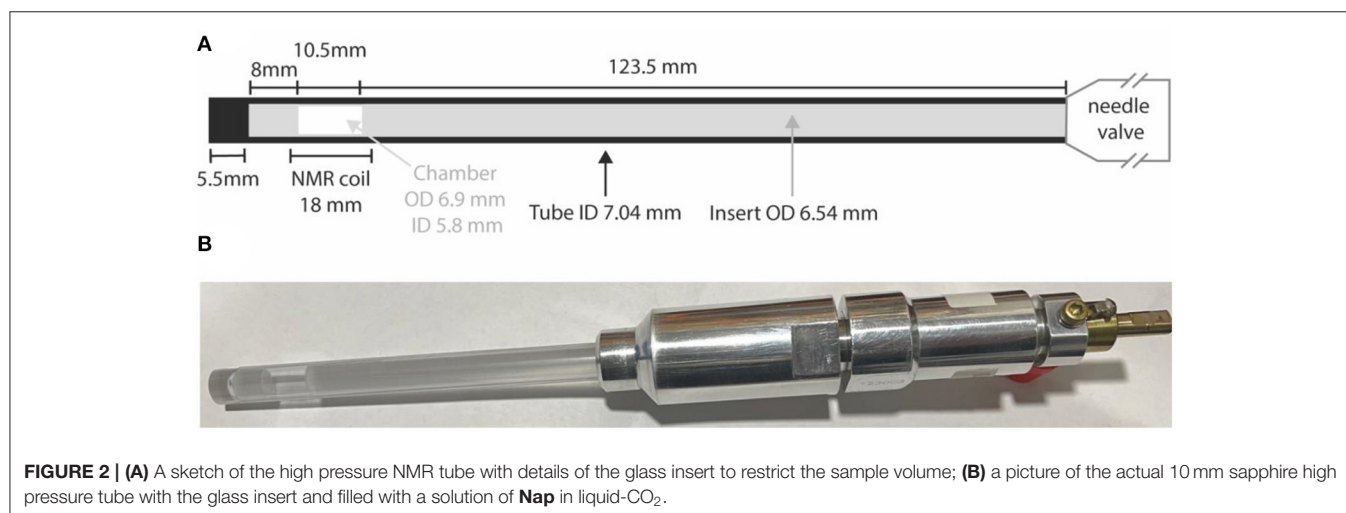

FIGURE 2 | (A) A sketch of the high pressure NMR tube with details of the glass insert to restrict the sample volume; (B) a picture of the actual 10 mm sapphire high pressure tube with the glass insert and filled with a solution of **Nap** in liquid-CO$_2$.

V_t is the total free volume in the tube which is the sum of the free volume of the chamber sitting in the middle of the coil plus the free volume in the gap between the tube inner walls and the insert. Since T, ρ_{gas}, ρ_{liq} and V_t are known we can set V_{liq} to match (or better to slightly exceed) the volume of the chamber placed in the NMR coil (V_C) and therefore work out the mass of CO$_2$ required. This mass is then calculated through the perfect gas law as:

$$M_{CO_2} = \frac{MW_{CO_2} \, P \, V_V}{R \, T} \qquad (4)$$

where R is the gas constant, P the pressure inside the vessel measured in our apparatus, and MW_{CO_2} the molecular weight of the gas. The required mass of CO$_2$ is then dispensed by adjusting the pressure inside the 50 ml vessel. The value of the pressure for the preparation below typically ranges between 2 and 8 bars. For practical purposes it was advantageous to charge an additional two bars of CO$_2$ (over the calculated value) into the 50 ml vessel.

This ensured that when the required CO$_2$ was removed from the vessel air was prevented from being drawn in, in the case of a leak, as the apparatus remained under two bars pressure.

As an illustrative example, to prepare sample **NapCo2e** in our 10 mm high-pressure sapphire tube with insert (see **Figure 2**) we have firstly calculated the tube free volume $V_t = 1098\,\mu l$ from known dimensions. Then, from tabulated values, we read $\rho_{gas} = 0.1942$ g/ml and $\rho_{liq} = 0.7734$ g/ml at the room temperature of 20°C. In this way, the mass of CO$_2$ that can be trapped in the 50 ml vessel at a pressure of 4.8 bar is $M_{CO_2} = 0.293$ g which gives a $\rho_{sys} = 0.394$ g/ml. This value is below the critical value and therefore the NMR tube will contain a mixture of liquid and gas. The volume of the liquid is calculated from Equation 1 to be $V_{liq} = 380\,\mu l$. Since the volume of the 10.5 mm chamber in the middle of the coil is $V_C = 280\,\mu l$, then the amount of liquid-CO$_2$ would fill the chamber and the gap above and below it for a few centimeters. To reach the concentration of 50 mM for this
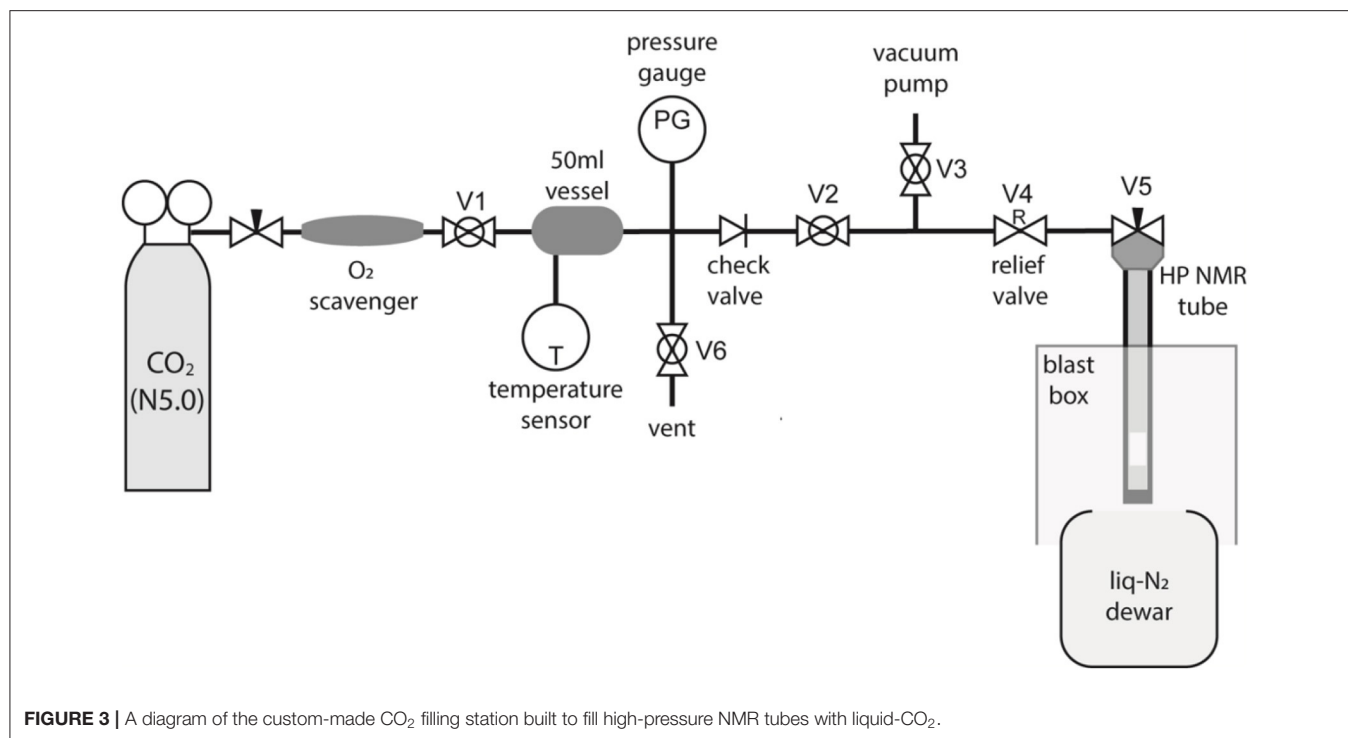
FIGURE 3 | A diagram of the custom-made CO$_2$ filling station built to fill high-pressure NMR tubes with liquid-CO$_2$.

sample, we have inserted 7.9 mg of **Nap** (MW $= 426.36$ g mol^{-1}). As discussed above we have therefore filled the 50 ml chamber with 6.8 bar of CO$_2$ gas and then transferred the gas into the NMR tube until the pressure reading was two bars.

Once the sample equilibrates at room temperature (20°C in our case), the approximate pressure inside the NMR tube can be estimated from the pressure-density phase diagrams of pure CO$_2$ (Smith et al., 2013) to be ~54 bars which is well within the tubes' tolerances (the value is only approximate because the phase diagram of our exact mixture is not available). Samples are moved around the laboratory within custom-made polycarbonate blast boxes and personnel wear face shields and gloves until the tube is safely placed into the probe.

NMR Procedures

All longitudinal decay constants (T$_1$) reported in this paper have been measured with a standard inversion recovery experiment. To measure singlet order decay constants (T$_S$) we have used a sequence (**Figure 4**) where firstly any singlet order possibly present in the sample from the previous scan is destroyed (Rodin et al., 2019), singlet order is subsequently produced with either a M2S (Pileio et al., 2010) or gM2S (Bengs et al., 2020) pulse sequence, depending on the actual spin system features. The singlet order is then allowed to relax in a specific magnetic field for some variable delay time before being reconverted back into transverse magnetization by a S2M or gS2M and acquired. A singlet filter block is inserted before the S2M/gS2M to filter through only singlet order. All measurements at fields below 7 T were performed in a field-cycling mode using a custom-made sample shuttle (Hall et al., 2020). In these experiments the sample is (*i*) polarized in high field; (*ii*) magnetization inverted with a 180 degrees pulse (for T$_1$) or converted to singlet order with a
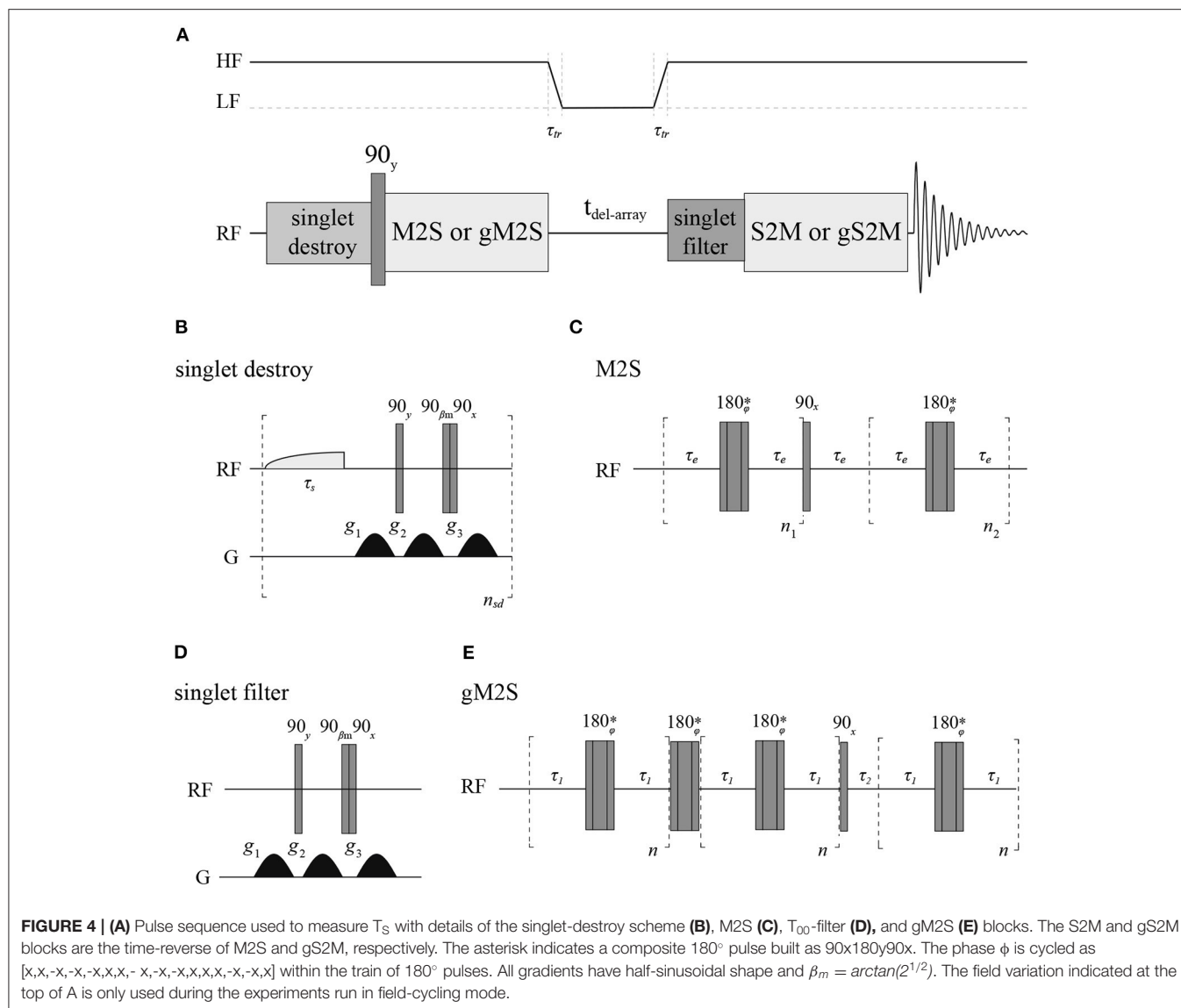
M2S or gM2S (for T$_S$); (*iii*) sample is moved to a region of lower field along the magnet vertical stray field where longitudinal or singlet order are let to decay; (*iv*) after a variable amount of time the sample is shuttled back into high field where a 90 degrees pulse (for T$_1$) or a S2M or gS2M are (for T$_S$) is applied before signal detection.

The duration of a 90 degrees ^{13}C pulse was 11.2, 25.0 and 27.5 µs at 16.4, 11.7 and 7 T, respectively, whereas the duration of the 90 degrees ^{1}H pulse was 9.5 µs at 7 T. Typically, for ^{13}C T$_1$ and T$_S$ experiments 8k points were collected using a 20 kHz spectral window. The recycling delay was fixed to 5T$_1$. The number of transients was set to two for all T$_1$ measurements and for T$_1$ and T$_S$ of **Mal**, **Act** and **Nap** in organic solvents whereas we have used four transients for T$_S$ measurements of Act and Nap in liquid-CO$_2$. The values of all parameters featuring in the pulse sequence of **Figure 4** have been optimized around their theoretical values and the results are summarized in **Table 2**. The gradients featuring in the singlet filter are applied along the z-axis and have strength of 75, -75 and -75 mT m^{-1} and durations of 2.4, 1.4, and 1 ms, respectively. The singlet destroy scheme has been implemented using a qramp shaped pulse of duration $\tau_s = 1$ s and maximum nutation frequency of 400 Hz. The sequence "shaped pulse-singlet filter" has been repeated n$_{sd} = 5$ times. In all field-cycling experiments the sample transport time τ_{tr} was set to 4 s.

EXPERIMENTAL

Naphthalene Derivative (Nap)

The naphthalene derivative (Hill-Cousins et al., 2015) (**Nap**) was chosen for initial investigations to develop and test the

FIGURE 4 | (A) Pulse sequence used to measure T$_S$ with details of the singlet-destroy scheme **(B)**, M2S **(C)**, T$_{00}$-filter **(D)**, and gM2S **(E)** blocks. The S2M and gS2M blocks are the time-reverse of M2S and gS2M, respectively. The asterisk indicates a composite 180° pulse built as 90x180y90x. The phase φ is cycled as [x,x,-x,-x,-x,x,x,- x, -x,-x,x,x,x,-x,-x,x] within the train of 180° pulses. All gradients have half-sinusoidal shape and $\beta_m = arctan(2^{1/2})$. The field variation indicated at the top of A is only used during the experiments run in field-cycling mode.

proposed procedures. The choice is based on the extraordinary long lifetime of the singlet order in this custom-designed and synthesized molecule (Stevanato et al., 2015; Hall et al., 2020).

Concentration Dependence of T$_1$ and T$_S$ in Liquid-CO$_2$ Solutions

The solubility of **Nap** in liquid-CO$_2$ was not known, nor was it known if sample concentration would affect the observed decay time. As a preliminary investigation a series of solutions of increasing concentrations of **Nap** in liquid-CO$_2$ at 20°C were prepared and T$_1$ and T$_S$ measured. Inspection of the results depicted in **Figure 5** reveals no significant trend in T$_1$ or T$_S$ with increasing concentration, it was concluded that a working concentration of 50 mM **Nap** in liquid-CO$_2$ was reasonable.
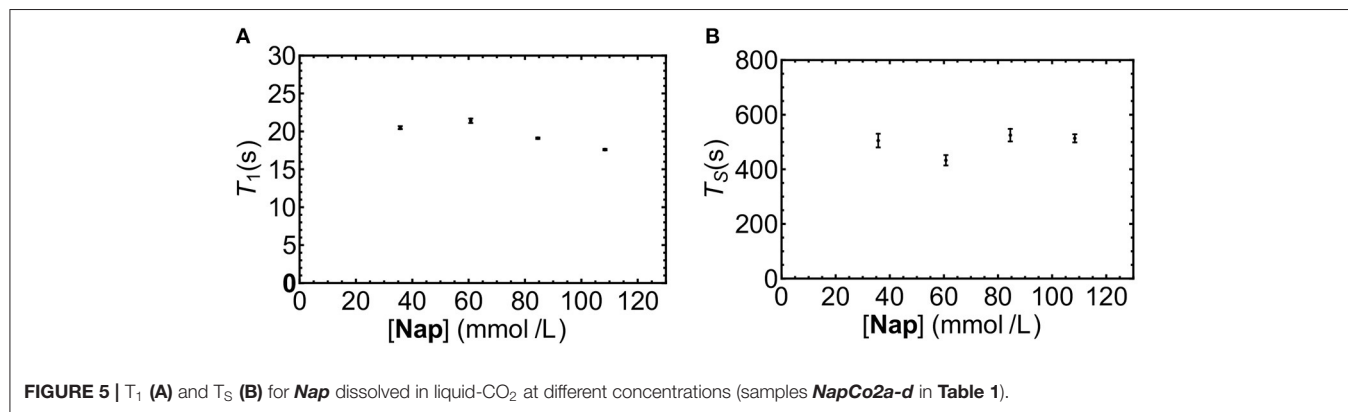
Viscosity Dependence of T$_1$ and T$_S$ in Liquid-CO$_2$ Solutions

To validate the initial hypothesis that both T$_1$ and T$_S$ can be prolonged in low-viscosity solutions, **Nap** was dissolved in a range of solvents of different viscosities from *tert*-butanol to liquid-CO$_2$. T$_1$ and T$_S$ were measured in samples **NapTbu, NapDms, NapEth, NapClf, NapMet, NapAce,** and **NapCo2e** and results from these experiments are summarized in **Figure 6**. These measurements have been taken at three different magnetic fields: 7 T (**Figure 6A**), 11.7 T (**Figure 6B**) and 16.4 T (**Figure 6C**).

Both T$_1$ and T$_S$ correlate linearly with inverse viscosity in common organic solvents at all three field strengths. At 16.4 T, the values of T$_1$ and T$_S$ measured in liquid-CO$_2$ solution (**NapCo2e**) also demonstrated a linear relationship with viscosity. Deviation from this behavior is observed at lower fields (**Figures 6A,B**) where the values of T$_1$ and T$_S$ for **NapCo2e** fail to meet the

TABLE 2 | Experimental values of the pulse sequence parameters used for the various samples in measuring T_S with the pulse sequence in **Figure 4**.

Sample	7 T			11.7 T			16.4 T		
	n_1	n_2	τ_e (ms)	n_1	n_2	τ_e (ms)	n_1	n_2	τ_e (ms)
NapTbu	14	7	4.6	8	4	4.6	6	3	4.6
NapDms	28	14	4.6	16	8	4.6	12	6	4.6
NapEth	16	8	4.6	10	5	4.6	6	3	4.6
NapClf	16	8	4.6	10	5	4.6	6	3	4.6
NapMet	16	8	4.6	10	5	4.6	6	3	4.6
NapAce	20	10	4.6	12	6	4.6	8	4	4.6
NapCo2e	22	11	4.6	12	6	4.6	8	4	4.6
MalEth	20	10	20.9						
MalCo2	44	22	20.9						
	n	τ_1 (ms)	τ_2 (ms)						
ActClf	3	1.10	0.7						
ActCo2	3	1.12	1.20						

FIGURE 5 | T_1 **(A)** and T_S **(B)** for **Nap** dissolved in liquid-CO_2 at different concentrations (samples **NapCo2a–d** in **Table 1**).
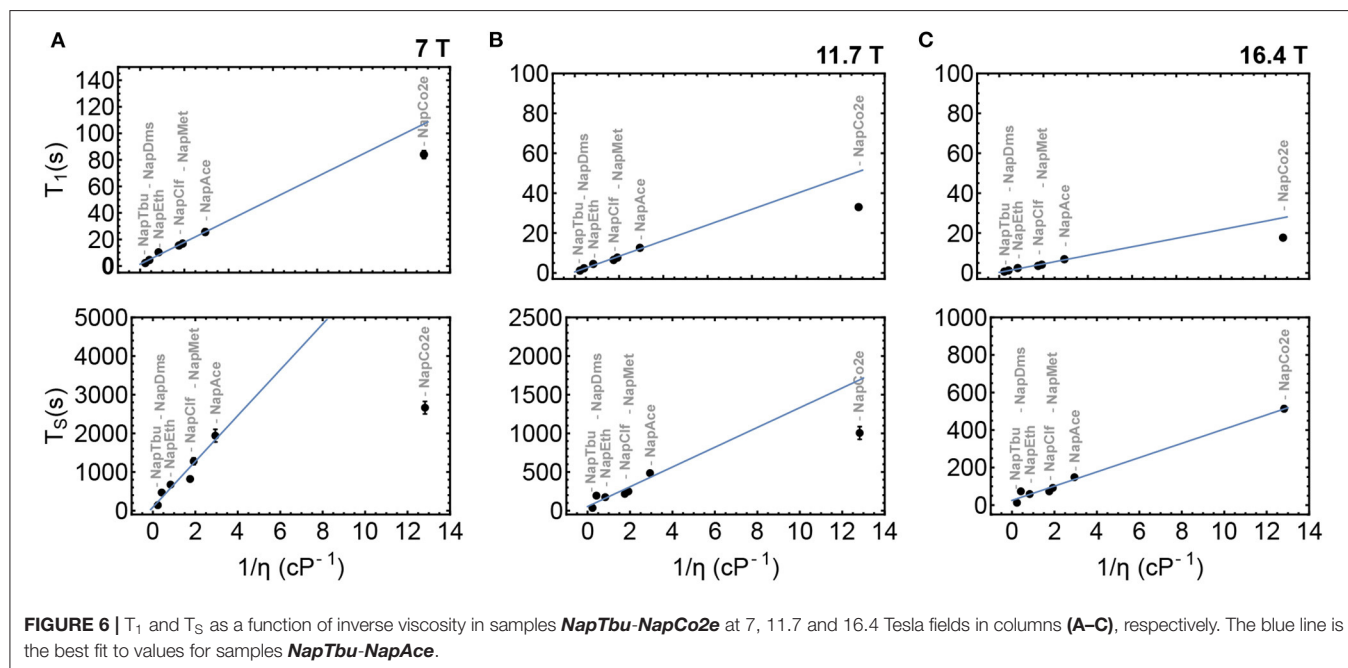
FIGURE 6 | T_1 and T_S as a function of inverse viscosity in samples **NapTbu-NapCo2e** at 7, 11.7 and 16.4 Tesla fields in columns **(A–C)**, respectively. The blue line is the best fit to values for samples **NapTbu-NapAce**.

predicted value (blue line), indicating that, although the values of T$_1$ and T$_S$ are significantly increased in liquid-CO$_2$, the time gain reduces as the magnetic field, at which relaxation occurs, reduces (**Figure 6**; **Table 3**).

Field Dependence of T$_1$ and T$_S$ in Liquid-CO$_2$ Solutions

The trends observed in **Figure 6** are evidence for the following: at the highest field, the relaxation of singlet order is dominated by chemical shift anisotropy, a mechanism whose contribution to the relaxation decay constant is directly proportional to inverse viscosity; as the field is lowered, the contribution to the relaxation rate from other mechanisms prevails, such mechanisms would therefore have a different proportionality to viscosity.

If this is the case, further reducing the field to a value where the chemical shift anisotropy contribution becomes negligible would make the T$_S$ in liquid-CO$_2$ fall below any recorded values. The same is not expected for T$_1$ as longitudinal order relaxation at any field would be dominated by the dipole-dipole mechanism whose contribution to the decay constant is inversely proportional to viscosity.

To investigate this hypothesis, we have measured the relaxation decay constants of longitudinal and singlet order at a range of fields between 50 mT and 7 T. Experiments were carried out in a field-cycling mode as described in Materials and Methods and for samples **NapEth, NapAce**, and **NapCo2e** where the labeled molecule **Nap** is dissolved in ethanol-d_6, acetone-d_6 and liquid-CO$_2$, respectively.

Close examination of the results of the field-cycling experiments (**Table 3**) reveals that the T$_1$ of all samples increases as the field is decreased (in all samples) indicating that the chemical shift anisotropy relaxation mechanism has a fundamental contribution to the observed decay constant at high field. However, at lower fields the T$_1$ values in liquid-CO$_2$ (**NapCo2e**) are significantly longer than those recorded in both ethanol-d_6 (**NapEth**) and acetone-d_6 (**NapAce**). The values of T$_1$ measured in liquid-CO$_2$ compared to ethanol-d_6 are extended by a factor of ∼7 at relatively high fields (16.4–7 T) but at lower fields this factor reduces to ∼5. When considering the sample in acetone-d_6 the extension factor is ∼2 at all fields.

A similar trend can be seen for T$_S$. The T$_S$ in liquid-CO$_2$ remains significantly longer than that measured in ethanol-d_6 at all fields, whereas in acetone-d_6, only at high fields the value of T$_1$ is significantly longer in liquid CO$_2$.

Interpreting our observations in a qualitative way, at high field, T$_1$ is dominated mainly by the interplay of ipDD and CSA mechanisms, so the value of T$_1$ increases as the CSA is progressively suppressed by transporting the sample to relax in a lower field. The contribution to the relaxation rate of both these mechanisms is expected to decrease as the viscosity reduces, explaining the significantly longer decay constants in liquid-CO$_2$ with respect to ethanol-d_6. The fall in lifetime extension of the liquid-CO$_2$ sample in comparison to ethanol-d_6 and acetone-d_6 as the field is lowered is due to the presence of a mechanism whose contribution becomes more relevant once the CSA becomes of less importance. The explanation is similar for the T$_S$ data, however, since singlet order is immune to the

ipDD mechanism, at high field the singlet order relaxation is mainly dominated by CSA whilst, other mechanisms become more important at lower field.

Acetylene Derivative (Act)

The field-cycling study to measure T$_1$ and T$_S$ as a function of magnetic field where relaxation occurs was repeated for the singlet-bearing acetylene derivative **Act** dissolved in CDCl$_3$ (**ActClf**) and in liquid-CO$_2$ (**ActCo2**) for comparison. Results from this study are summarized in **Table 4**.

Again, both T$_1$ and T$_S$ increased as the field decreased, once more pointing toward a substantial role of CSA in the relaxation mechanism at high field. However, the T$_1$ reaches a maximum at 3 T and then slowly diminishes again toward lower fields. There is a clear time gain of a factor of 3-4 approximately in longitudinal order lifetime when using liquid-CO$_2$ as a solvent in comparison to CDCl$_3$. Interestingly, T$_S$ shows a significant gain of a factor of ∼4 in liquid-CO$_2$ (from 7 T down to 3 T) but this factor diminishes and even inverts at lower fields, with the T$_S$ in CDCl$_3$ being longer than that measured in liquid-CO$_2$ in very low field.

Maleate Derivative (Mal)

In a third set of field-cycling experiments the T$_1$ and T$_S$ of molecule **Mal** was measured at a range of magnetic fields both in ethanol-d_6 (**MalEth**) and liquid-CO$_2$ (**MalCo2**). Results from this study are summarized in **Table 5**. In this sample the singlet order is created in the proton spin-pair and protons have notoriously much smaller chemical shift tensors than carbons. For this reason, it is not expected that the CSA relaxation mechanism contributes significantly to the total relaxation decay at any magnetic field. Indeed, from the data in the table the values of both T$_1$ and T$_S$ in either sample do not vary significantly as the field is lowered. Comparing the results in liquid-CO$_2$ with those in ethanol-d_6, a gain by a factor ∼4 is observed for T$_1$ but there is a more modest gain factor of ∼1.4 observed for T$_S$.

DISCUSSION

The data presented above can be interpreted using a relaxation analysis based on previously derived analytical equations for the contribution of different mechanisms to the total relaxation rate of singlet spin order (Pileio, 2010, 2020). To do so, it is better to discuss in terms of decay rates $R_1 = 1/T_1$ and $R_S = 1/T_S$ since the contributions of different relaxation mechanisms to the rate is additive. Additionally, we are going to use a simplified model where only the intrapair dipole-dipole (ipDD), chemical shift anisotropy (CSA) and the coherent chemical shift leak (CSL) mechanism are explicitly introduced. The remaining contribution to the total decay rate will be introduced as an unknown mechanism and its value retrieved through data fitting.

The equations for the decay rates due to the cited mechanism have been largely discussed in literature (Pileio, 2020) and are

TABLE 3 | T_1 and T_S values for samples **NapEth**, **NapAce,** and **NapCo2e** obtained at 20°C and different magnetic field strengths.

Field (T)	T_1 (s)			T_S (s)		
	NapEth	**NapAce**	**NapCo2e**	**NapEth**	**NapAce**	**NapCo2e**
0.05	26 ± 2	72 ± 3	135 ± 26	1,350 ± 98	5,319 ± 682	4,553 ± 470
0.10	33 ± 5	75 ± 5	126 ± 18	1,587 ± 130	4,454 ± 369	*
0.25	25 ± 1	92 ± 11	176 ± 12	1,573 ± 70	4,460 ± 369	3,785 ± 318
0.5	30 ± 4	80 ± 5	158 ± 14	1,503 ± 52	5,146 ± 484	3,266 ± 192
1	32 ± 3	80 ± 8	148 ± 20	1,426 ± 76	5,075 ± 363	3,171 ± 153
2	30 ± 4	70 ± 10	175 ± 18	1,556 ± 21	4,429 ± 381	*
3	27 ± 1	57 ± 3	122 ± 7	1,291 ± 62	3,852 ± 302	2,851 ± 105
7	10 ± 1	30 ± 1	84 ± 3	620 ± 30	1,621 ± 208	2,664 ± 161
11.7	4.5 ± 0.1	16 ± 1	33 ± 1	174 ± 2	485 ± 16	1,005 ± 82
16.4	2.5 ± 0.1	7 ± 0.2	18 ± 0.1	59 ± 1	148 ± 5	513 ± 15

*Data not collected.

TABLE 4 | T_1 and T_S values for samples **ActClf** and **ActCo2** obtained at 20°C and different magnetic field strengths.

Field (T)	T_1 (s)		T_S (s)	
	ActClf	**ActCo2**	**ActClf**	**ActCo2**
0.05	34 ± 1	96 ± 2	4,123 ± 260	2,605 ± 258
0.10	32 ± 1	102 ± 9	3,675 ± 320	*
0.25	36 ± 2	127 ± 6	3,077 ± 300	*
0.5	37 ± 2	120 ± 5	2,914 ± 156	2,611 ± 82
1	41 ± 1	146 ± 12	1,468 ± 56	2,450 ± 120
3	47 ± 3	132 ± 8	214 ± 20	805 ± 78
5	35 ± 2	114 ± 6	100 ± 8	*
7	20 ± 1	78 ± 3	54 ± 6	218 ± 17

*Data not collected.

reported here for convenience:

$$R_1^{ipDD} = \frac{3}{2}b_{jk}^2\tau_2; \quad R_S^{ipDD} = 0$$

$$R_1^{CSA^+} = \frac{1}{10}\gamma^2 B_0^2 \tau_2 \left(\left\| \delta_{\mathbf{j}}^+ \right\|^2 + \left\| \delta_{\mathbf{k}}^+ \right\|^2 \right);$$

$$R_S^{CSA^+} = \frac{2}{9}\gamma^2 B_0^2 \tau_2 \left\| \delta_{\mathbf{j}}^+ - \delta_{\mathbf{k}}^+ \right\|^2$$

$$R_1^{CSA^-} = \frac{1}{6}\gamma^2 B_0^2 \tau_1 \left(\left\| \delta_{\mathbf{j}}^- \right\|^2 + \left\| \delta_{\mathbf{k}}^- \right\|^2 \right);$$

$$R_S^{CSA^-} = \frac{2}{9}\gamma^2 B_0^2 \tau_1 \left\| \delta_{\mathbf{j}}^- - \delta_{\mathbf{k}}^- \right\|^2$$

$$R_1^{CSL} = 0; \quad R_S^{CSL} = \frac{\gamma^2 B_0^2 \Delta\delta_{iso}^2 \tau_2 b_{jk}^2}{12\pi^2 J_{jk}^2} \quad (5)$$

where $b_{jk} = -\hbar\mu_0\gamma^2/(4\pi r_{jk}^3)$ and J_{jk} are, respectively, the dipolar and indirect coupling constants between the two nuclei in the singlet spin-pair; B_0 is the static magnetic field, $\Delta\delta_{iso} = \delta_j - \delta_k$ is the difference in the chemical shift of the two nuclei; τ_1 and τ_2 are the correlation times for rank-1 and rank-2 mechanisms, respectively and with $\tau_1 = 3\tau_2$; γ is the gyromagnetic ratio; δ^+ and δ^- are the symmetric (+) and asymmetric (−) parts of the

chemical shift tensor for the two nuclei in the singlet pair; $\|\delta\|$ indicates the Frobenius norm of the tensor δ.

The strategy adopted is based on the following assumptions:

- T_1 in low field is dominated by the ipDD mechanism only, thus we can use R_1^{ipDD} and the experimental value of T_1 at 50 mT to retrieve the correlation time (other spin system parameters reported in **Table 6**)

$$\tau_2 = \frac{2}{3b_{jk}^2 T_1(50mT)} \quad (6)$$

- T_1 at any other field is due to the effect of ipDD and CSA mechanisms:

$$T_1 = 1/(R_1^{ipDD} + R_1^{CSA^+} + R_1^{CSA^-}) \quad (7)$$

- T_S at all fields is due to the combination of CSA and CSL terms plus a further mechanism whose rate R_S^X will be determined by fitting the experimental T_S:

Field (T)	T$_1$ (s)		T$_S$ (s)	
	MalEth	**MalCo2**	**MalEth**	**MalCo2**
0.05	9.6 ± 0.1	37.6 ± 0.4	237 ± 2	294 ± 8
0.10	9.5 ± 0.2	37.6 ± 0.3	233 ± 2	325 ± 20
0.25	9.7 ± 0.2	39.2 ± 0.4	251 ± 4	327 ± 15
0.5	9.7 ± 0.2	39.4 ± 0.5	249 ± 6	344 ± 22
1	9.8 ± 0.2	41.2 ± 0.3	250 ± 6	376 ± 21
3	9.5 ± 0.1	43.8 ± 0.5	246 ± 9	364 ± 15
5	9.8 ± 0.1	44.3 ± 0.8	237 ± 8	331 ± 15
7	9.7 ± 0.1	43.8 ± 1.6	242 ± 6	359 ± 27

TABLE 6 | Parameters used in the relaxation analysis for the case of **NapAce** and **NapCo2e**.

Parameter	NapAce	NapCo2e
r_{jk}	1.395 Å	1.395 Å
J_{jk}	54.8 Hz	54.8 Hz
$\Delta\delta_{iso}$	0.057 ppm	0.052 ppm
$\left\|\delta_{\mathbf{j}}^{+}\right\|$		107 ppm
$\left\|\delta_{\mathbf{k}}^{+}\right\|$		112 ppm
$\left\|\delta_{\mathbf{j}}^{-}\right\|$		2.6 ppm
$\left\|\delta_{\mathbf{k}}^{-}\right\|$		8.1 ppm
$\left\|\delta_{\mathbf{j}}^{+}-\delta_{\mathbf{k}}^{+}\right\|$		6.7 ppm
$\left\|\delta_{\mathbf{j}}^{-}-\delta_{\mathbf{k}}^{-}\right\|$		9.9 ppm

Chemical shift tensors have been calculated in Stevanato et al. (2015) and here are assumed identical for both samples.

$$T_S = 1/(R_S^{CSA^+} + R_S^{CSA^-} + R_S^{CSL} + R_S^{X}) \qquad (8)$$

In the case of sample **NapAce** and using Equation 6 we find a correlation time $\tau_2 = 31$ ps which can then be used to predict the value of T$_1$ and T$_S$ at any field. The values of T$_1$ predicted using Equation 7 are plotted as a continuous line in **Figure 7A** and overlapped with the experimental point of **Table 3** for an easy comparison. In the case of T$_S$ we have fitted the experimental data against Equation 8 and for the unknown R_S^X which was found to be 198.5 × 10^{-6} s^{-1}. The fitting is shown in **Figure 7B**.

The same procedure was used to predict the values of T$_1$ and T$_S$ for the sample of **Nap** in liquid-CO$_2$ (**NapCo2e**). In this case and using Equation 6 we found a value of the correlation time of $\tau_2 = 16$ ps and the fitted value of R_S^X was found to be 268.3 × 10^{-6} s^{-1}. The predicted values for this case are shown in **Figures 7C,D** for T$_1$ and T$_S$, respectively.

The results of this approximate relaxation analysis can be summarized as follows: in agreement with the initial hypothesis, the T$_1$ of these samples is essentially defined by the ipDD and CSA relaxation terms since the predicted values matches well the experimental points; in the case of T$_S$, relaxation in low fields is governed by a mechanism that contributes

with a rate of 195.5 × 10^{-6} for the case of **Nap** in acetone-d$_6$ and 268.3 × 10^{-6} for the case of **Nap** in liquid-CO$_2$. This additional mechanism seems to have less dependence on viscosity than ipDD or CSA since its value is higher in the less viscous liquid-CO$_2$ sample. One possible candidate is the spin-rotation mechanism whose dependence on the solvent viscosity is opposite to that of ipDD and CSA. Indeed, a variant of the spin-rotation mechanism, known as spin-internal motion (SIM), has already been proposed as an important relaxation mechanism for the singlet spin order of **Nap** in a previous study (Stevanato et al., 2015).

CONCLUSION

In this study we have run a thorough investigation of the lifetime of both longitudinal and singlet order decay times of three different molecules in liquid-CO$_2$ solutions in comparison with the values measured in more common organic solvents. The motivation behind this work was the concept that longitudinal and singlet order lifetimes could be extended in low viscosity compressed gases in comparison to solvents which are liquid at ordinary pressures and temperatures. Significantly, we have shown that liquid-CO$_2$ allows an extension of lifetime of at least two-fold when compared with lifetime available in acetone-d$_6$, one of the lowest viscosity solvents available. However, and depending on the relaxation mechanisms acting, such gain may not be able to prolong the absolute lifetime of singlet order since the latter hits a plateau where relaxation seems to be dominated by mechanisms that do not necessarily benefit from the lower viscosity of the liquid-CO$_2$ solution.

Nevertheless, the possibility to store spin polarization (and hence hyperpolarization) for as long as 76 min, in the case of **NapCo2e,** at 50 mT, but in a solvent which can be removed almost instantaneously by simply opening the tube, suggests the possibility of new exciting experiments. Experiments where hyperpolarization is stored for tens of minutes in a substrate dissolved in liquid-CO$_2$ and retrieved, at the time of use, by quick evaporation followed by dissolution in an experiment-compatible solvent which
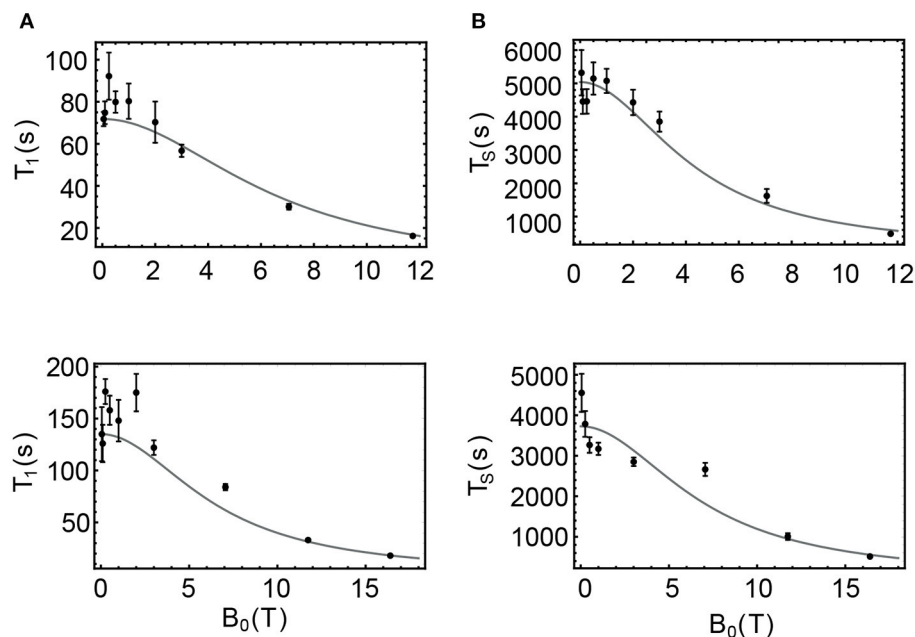
FIGURE 7 | Filled circles are the values of T_1 and T_S experimentally measured for samples ***NapAce* (A,B)** and ***NapCo2e* (C,D)**, also available in **Table 3**. The gray curves are the predicted values of these decay constants obtained using Equations 5–8.

is perhaps not very convenient for hyperpolarization storage. We are currently building equipment to verify this hypothesis.

DATA AVAILABILITY STATEMENT

The original contributions presented in the study are included in the article/supplementary material, further inquiries can be directed to the corresponding author/s.

AUTHOR CONTRIBUTIONS

FUNDING

ACKNOWLEDGMENTS

REFERENCES

Adams, R. W., Aguilar, J. A., Atkinson, K. D., Cowley, M. J., Elliott, P. I., Duckett, S. B., et al. (2009). Reversible interactions with para-hydrogen enhance NMR sensitivity by polarization transfer. *Science.* 323, 1708–1711. doi: 10.1126/science.1168877

Ahuja, P., Sarkar, R., Vasos, P. R., and Bodenhausen, G. (2009). Diffusion coefficients of biomolecules using long-lived spin states. *J. Am. Chem. Soc.* 131, 7498–7499. doi: 10.1021/ja902030k

Ardenkjaer-Larsen, J. H., Fridlund, B., Gram, A., Hansson, G., Hansson, L., Lerche, M. H., et al. (2003). Increase in signal-to-noise ratio of > 10,000 times in liquid-state NMR. *Proc. Natl. Acad. Sci. USA.* 100, 10158–10163. doi: 10.1073/pnas.1733835100

Bai, S., Taylor, C. M. V., Liu, F., Mayne, C. L., Pugmire, R. J., and Grant, D. M. (1997). CO$_2$ clustering of 1-decanol and methanol in supercritical fluids by 13C nuclear spin–lattice relaxation. *J. Phys. Chem. B.* 101, 2923–2928. doi: 10.1021/jp9640484

Bengs, C., Sabba, M., Jerschow, A., and Levitt, M. H. (2020). Generalised magnetisation-to-singlet-order transfer in nuclear magnetic resonance. *Phys. Chem. Chem. Phys.* 22, 9703–9712. doi: 10.1039/D0CP00935K

Bowers, C. R., and Weitekamp, D. P. (1987). Parahydrogen and synthesis allow dramatically enhanced nuclear alignment. *J. Am. Chem. Soc.* 109, 5541–5542. doi: 10.1021/ja00252a049

Brown, L. J. (2020). Design synthesis of molecules supporting long-lived spin order. In: *Long-Lived Nuclear Spin Order: Theory Applications.* Ed G. Pileio. London: Royal Society of Chemistry. doi: 10.1039/9781788019972-00093

Buratto, R., Mammoli, D., Chiarparin, E., Williams, G., and Bodenhausen, G. (2014). Exploring weak ligand–protein interactions by long-lived NMR States: improved contrast in fragment-based drug screening. *Angew. Chem. Int. Ed.* 53, 11376–11380. doi: 10.1002/anie.201404921

Carravetta, M., Johannessen, O. G., and Levitt, M. H. (2004). Beyond the T1 limit: singlet nuclear spin states in low magnetic field. *Phys. Rev. Letts.* 92:153003. doi: 10.1103/PhysRevLett.92.153003

Carravetta, M., and Levitt, M. H. (2004). Long-lived nuclear spin states in high-field solution NMR. *J. Am. Chem. Soc.* 126, 6228–6229. doi: 10.1021/ja0490931

Cavadini, S., Dittmer, J., Antonijevic, S., and Bodenhausen, G. (2005). Slow diffusion by singlet state NMR spectroscopy. *J. Am. Chem. Soc.* 127, 15744–15748. doi: 10.1021/ja052897b

DeVience, S. J., Walsworth, R. L., and Rosen, M. S. (2013). Nuclear spin singlet states as a contrast mechanism for NMR spectroscopy. *NMR Biomed.* 26, 1204–1212. doi: 10.1002/nbm.2936

Dumez, J. N., Håkansson, P., Mamone, S., Meier, B., Stevanato, G., Hill-Cousins, J. T., et al. (2015). Theory of long-lived nuclear spin states in methyl groups and quantum-rotor induced polarisation. *J. Chem. Phys.* 142:044506. doi: 10.1063/1.4906273

Dumez, J. N., Hill-Cousins, J. T., Brown, R. C. D., and Pileio, G. (2014). Long-lived localization in magnetic resonance imaging. *J. Magn. Reson.* 246, 27–30. doi: 10.1016/j.jmr.2014.06.008

Feng, Y., Theis, T., Liang, X., Wang, Q., Zhou, P., and Warren, W. S. (2013). Storage of hydrogen spin polarization in long-lived $^{13}C_2$ singlet order and implications for hyperpolarized magnetic resonance imaging. *J. Am. Chem. Soc.* 135, 9632–9635. doi: 10.1021/ja404936p

Gaemers, S., and Elsevier, C. J. (2000). 14N NMR spectroscopy of tertiary amines in supercritical fluids. *Magn. Reson. Chem.* 38, 650–654. doi: 10.1002/1097-458X(200008)38:8<650::AID-MRC705>3.0.CO;2-U

Gaemers, S., Elsevier, C. J., and Bax, A. (1999). NMR of biomolecules in low viscosity, liquid CO_2. *Chem. Phys. Lett.* 301, 138–144. doi: 10.1016/S0009-2614(99)00012-3

Gajan, D., Bornet, A., Vuichoud, B., Milani, J., Melzi, R., van Kalkeren, H. A., et al. (2014). Hybrid polarizing solids for pure hyperpolarized liquids through dissolution dynamic nuclear polarization. *Proc. Natl. Acad. Sci. USA.* 111, 14693–14697. doi: 10.1073/pnas.1407730111

Hall, A. M. R., Cartlidge, T. A. A., and Pileio, G. (2020). *A temperature-controlled sample shuttle for field-cycling NMR. J. Magn. Reson.* 317:106778. doi: 10.1016/j.jmr.2020.106778

Hill-Cousins, J. T., Pop, I. A., Pileio, G., Stevanato, G., Hakansson, P., Roy, S. S., et al. (2015). Synthesis of an isotopically labeled naphthalene derivative that supports a long-lived nuclear singlet state. *Org. Lett.* 17, 2150–2153. doi: 10.1021/acs.orglett.5b00744

Khodov, I., Dyshin, A., Efimov, S., Ivlev, D., and Kiselev, M. (2020). High-pressure NMR spectroscopy in studies of the conformational composition of small molecules in supercritical carbon dioxide. *J Mol Liquids.* 309:113113. doi: 10.1016/j.molliq.2020.113113

Kowalewski, J., and Mäler, L. (2006). *Nuclear Spin Relaxation in Liquids: Theory, Experiments and Applications.* Boca Raton, FL: CRC Press/Taylor & Francis Group. doi: 10.1201/9781420012194

Lamb, D. M., Adamy, S. T., Woo, K. W., and Jonas, J. (1989). Transport and relaxation of naphthalene in supercritical fluids. *J. Phys. Chem.* 93, 5002–5005. doi: 10.1021/j100349a065

Levitt, M. H. (2012). Singlet nuclear magnetic resonance. *Annu. Rev. Phys. Chem.* 63, 89–105. doi: 10.1146/annurev-physchem-032511-143724

Mamone, S., and Glöggler, S. (2018). Nuclear spin singlet states as magnetic on/off probes in self-assembling systems. *Phys. Chem. Chem. Phys.* 20, 22463–22467. doi: 10.1039/C8CP04448A

Pileio, G. (2010). Relaxation theory of nuclear singlet states in two spin-1/2 systems. *Prog Nuclear Magn Reson Spectroscopy.* 56, 217–231. doi: 10.1016/j.pnmrs.2009.10.001

Pileio, G. (2020). Long-lived nuclear spin order: theory and applications. In: *New Developments in NMR. Ed W. Price. Royal Society of Chemistry.* London: Royal Society of Chemistry. doi: 10.1039/9781788019972

Pileio, G., Carravetta, M., and Levitt, M. H. (2010). Storage of nuclear magnetization as long-lived singlet order in low magnetic field. *Proc. Natl. Acad. Sci. USA.* 107:17135–17139. doi: 10.1073/pnas.1010570107

Pileio, G., Hill-Cousins, J. T., Mitchell, S., Kuprov, I., Brown, L. J., Brown, R., et al. (2012). Long-lived nuclear singlet order in near-equivalent 13C spin pairs. *J. Am. Chem. Soc.* 134, 17494–17497. doi: 10.1021/ja3089873

Pileio, G., J.-,Dumez, N., I.-,Pop, A., Hill-Cousins, J. T., and Brown, R. C. D. (2015). Real-space imaging of macroscopic diffusion slow flow by singlet tagging MRI. *J. Magn. Reson.* 252, 130–134. doi: 10.1016/j.jmr.2015.01.016

Pileio, G., and Ostrowska, S. (2017). Accessing the long-time limit in diffusion NMR: the case of singlet assisted diffusive diffraction q-space. *J. Magn. Reson.* 285, 1–7. doi: 10.1016/j.jmr.2017.10.003

Rodin, B. A., Sheberstov, K. F., Kiryutin, A. S., Brown, L. J., Brown, R. C. D., Sabba, M., et al. (2019). Fast destruction of singlet order in NMR experiments. *J. Chem. Phys.* 151:234203. doi: 10.1063/1.5131730

Salvi, N., Buratto, R., Bornet, A., Ulzega, S., Rentero Rebollo, I., Angelini, A., et al. (2012). Boosting the sensitivity of ligand-protein screening by NMR of long-lived states. *J. Am. Chem. Soc.* 134, 11076–11079. doi: 10.1021/ja303301w

Saul, P., Mamone, S., and Glöggler, S. (2019). Nuclear singlet multimers (NUSIMERs) with long-lived singlet states. *Chem. Sci.* 10, 413–417. doi: 10.1039/C8SC02831A

Smith, R., Inmate, H., and Peters, C. (2013). *Introduction to supercritical fluids, a spreadsheets based* approach. In: Supercritical Fluids Science and Technology. Oxford, UK: Elsevier Science & Technology.

Stevanato, G., Hill-Cousins, J. T., Håkansson, P., Roy, S. S., Brown, L. J., Brown, R. C. D., et al. (2015). A nuclear singlet lifetime of more than one hour in room-temperature solution. *Angew. Chem. Int. Ed.* 54, 3740–3743. doi: 10.1002/anie.201411978

Tanner, C. P. N., Lindale, J. R., Eriksson, S. L., Zhou, Z., Colell, J. F. P., Theis, T., et al. (2019). Selective hyperpolarization of heteronuclear singlet states via pulsed microtesla SABRE. *J. Chem. Phys.* 151:044201. doi: 10.1063/1.5108644

Theis, T., Ortiz, G. X., Logan, A. W., Claytor, K. E., Feng, Y., Huhn, W. P., et al. (2016). and cost-efficient hyperpolarization of long-lived nuclear spin states on universal (15)N2-diazirine molecular tags. *Sci Adv.* 2:e1501438. doi: 10.1126/sciadv.1501438

Tourell, M. C., Pop, I. A., Brown, L. J., Brown, R. C. D., and Pileio, G. (2018). Singlet-assisted diffusion-NMR (SAD-NMR): redefining the limits when measuring tortuosity in porous media. *Phys. Chem. Chem. Phys.* 20, 13705–13713. doi: 10.1039/C8CP00145F

Yang, S., McCormick, J., Mamone, S., Bouchard, L. S., and Glöggler, S. (2019). Nuclear spin singlet states in photoactive molecules: from fluorescence/NMR bimodality to a bimolecular switch for spin singlet states. *Angew. Chem. Int. Ed.* 58, 2879–2883. doi: 10.1002/anie.201814198

Yonker, C. R. (2000). Solution dynamics of perfluorobenzene, benzene, and perdeuteriobenzene in carbon dioxide as a function of pressure and temperature. *J. Phys. Chem. A.* 104, 685–691. doi: 10.1021/jp992725z

Zhang, Y., Basu, K., Canary, J. W., and Jerschow, A. (2015). Singlet lifetime measurements in an all-proton chemically equivalent spin system by hyperpolarization and weak spin lock transfers. *Phys. Chem. Chem. Phys.* 17, 24370–24375. doi: 10.1039/C5CP03716F

Zhang, Y., Duan, X., Soon, P. C., Sychrovsk,ý V., Canary, J. W., and Jerschow, A. (2016). Limits in proton nuclear singlet-state lifetimes measured with para-hydrogen-induced polarization. *ChemPhysChem.* 17, 2967–2971. doi: 10.1002/cphc.201600663

Zhang, Y. N., Soon, P. C., Jerschow, A., and Canary, J. W. (2014). Long- lived 1H nuclear spin singlet in dimethyl maleate revealed by addition of thiols. *Angew. Chem. Int. Ed.* 53, 3396–3399. doi: 10.1002/anie.201310284